MECHATRONIC POWERTRAIN VIRTUAL SENSOR: SYSTEM-LEVEL MODEL AND SENSOR SELECTION

Rottiers, W. [1,2], Naets, F.[1,2], Forrier, B.[1,2], Sarrazin, M.[3], Van der Auweraer, H.[3] and Desmet, W.[1,2]

[1] *Department of Mechanical Engineering, KU Leuven,*
Celestijnenlaan 300, 3001 Heverlee, Belgium.
ward.rottiers@kuleuven.be

[2] *Member of Flanders Make*

[3] *Siemens Industry Software NV,*
Interleuvenlaan 68, 3001 Heverlee, Belgium.

ABSTRACT
Virtual sensors provide measurements for variables and parameters which are difficult to measure, based on a small number of (preferably pragmatic) measurements in combination with a numerical model of the observed system. This work presents a global virtual sensor to extract the full state of a mechatronic drivetrain based on a system-level model and a Kalman filter. Sensor selection is performed based on an observability analysis and the Kalman filter settings are based on a Monte-Carlo simulation. The virtual sensor is validated experimentally on a mechatronic powertrain test setup.

KEYWORDS: Multisensor integration, Mechatronics, State estimation, Dynamic models, Kalman filters

1. INTRODUCTION

In mechatronic applications, the measurement of all operational quantities of interest is practically unfeasible. Virtual sensing combines a small number of preferably non-intrusive and cheap measurements to determine the complete state of a numerical model describing the observed system [1].
Problem specific applications of virtual sensing or state estimation are discussed in a range of works. [2] applies an extended Luenberger observer and [3] applies Kalman filtering with a range of different models, as discussed by [3, 4, 5]. The observability of these models are in many cases investigated [2], [6]. Classically, virtual sensors have been applied in applications with relatively large time constants, like bio reactors, and have more recently found entry in the field of mecha(tro)nics which operate at much higher frequencies.
This work discusses the design and validation of a virtual sensor for a mechatronic drivetrain. The proposed approach exploits a multi-physical system-level model of the drivetrain which allows the integration of information coming from electrical and mechanical sensors. Due to it's low computational load, a nonlinear Kalman filtering approach is used to combine the model and sensor information. A detailed observability analysis is performed to not only determine the necessary sensors, but also the best sensors from a given set of possible sensors. Experimental results are provided to investigate the accuracy of the resulting virtual sensor.

2. MECHATRONIC POWERTRAIN OVERVIEW

The global layout of the mechatronic powertrains considered in this work is shown in Fig. 1. This architecture was proposed by [7] for a test-setup to validate virtual sensor approaches.
The powertrain consists of two induction motors interconnected by a cardanic shaft with nonlinear kinematics. Since one motor can act as a variable load, the setup represents the global layout of many real-world machines.

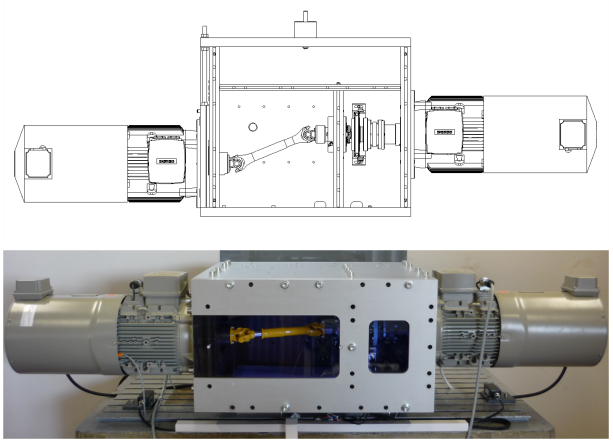

Figure 1 – CAD-design and photo of mechatronic powertrain proposed by [7].

3. NON-LINEAR POWERTRAIN MODEL

The multiphysical system-level mechatronic drivetrain model consists of a mechanical and electric model which are combined. Both models are discussed in the following sections.

3.1. Mechanical model

The cardan shaft consists of two Hooke's joints, which are able to connect two non-coaxial shafts. The kinematic relation between the rotation angle θ of the in- and outgoing axles (respectively a and b) for a shaft under a deflection angle β is:

$$\theta_b = \arctan\left(\frac{\tan(\theta_a)}{\cos(\beta)}\right) = f_\theta\left(\theta_a(t), \beta\right). \tag{1}$$

The kinematics of a cardan shaft with coplanar yokes is given by:

$$\tan\theta_2 = \frac{cos\beta_1 tan\theta_1}{\cos\beta_2}. \tag{2}$$

Consequently, the equality of the deflection angles $\beta_1 = \beta_2$ is a sufficient condition for a synchronous movement at both ends of the cardan shaft, as discussed by [8].
A lumped parameter model (Fig. 2) is used to describe the dynamic torsional behavior of the mechanical transmission. The model considers lossless Hooke's joints:

$$\dot{\theta}_i T_{\theta_i} + \dot{\theta}_{\mathfrak{c}_i} T_{\mathfrak{c}_i} = 0. \tag{3}$$

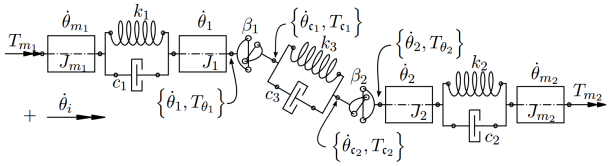

Figure 2 – Basic lumped parameter, dynamic model of the mechanical part of the drivetrain.

The intermediate shaft of the dynamic model is flexible which results in loss of the synchronization. This is modeled through a simple mass-spring relation, as shown in Fig. 2. The equations of motion for the flexible shaft model

are:

$$\dot{\mathbf{x}} = \left\{ \begin{array}{l} \dot{\theta}_{m_1} \\ J_{m_1}^{-1} \left(-c_1 \left(\dot{\theta}_{m_1} - \dot{\theta}_1 \right) - k_1 (\theta_{m_1} - \theta_1) + T_{m_1} \right) \\ \dot{\theta}_1 \\ J_1^{-1} \left(c_1 \left(\dot{\theta}_{m_1} - \dot{\theta}_1 \right) + k_1 (\theta_{m_1} - \theta_1) - T_{\theta_1} \right) \\ \dot{\theta}_2 \\ J_2^{-1} \left(c_2 \left(\dot{\theta}_{m_2} - \dot{\theta}_2 \right) + k_2 \left(\theta_{m_2} - \theta_2 \right) - T_{\theta_2} \right) \\ \dot{\theta}_{m_2} \\ J_{m_2}^{-1} \left(-c_2 \left(\dot{\theta}_{m_2} - \dot{\theta}_2 \right) - k_2 (\theta_{m_2} - \theta_2) + T_{m_2} \right) \end{array} \right\}, \tag{4}$$

$$T_{\theta_1} = \left(c_3 \left(\dot{\theta}_{c_1} - \dot{\theta}_{c_2} \right) + k_3 \left(\theta_{c_1} - \theta_{c_2} \right) \right) \frac{\cos(\beta_1)}{1 - \sin^2(\beta_1)\cos^2(\theta_1)}, \tag{5}$$

$$T_{\theta_2} = \left(-c_3 \left(\dot{\theta}_{c_1} - \dot{\theta}_{c_2} \right) - k_3 \left(\theta_{c_1} - \theta_{c_2} \right) \right) \frac{\cos(\beta_2)}{1 - \sin^2(\beta_2)\cos^2(\theta_2)}, \tag{6}$$

with state vector $\mathbf{x} = \left\{ \theta_{m_1}, \dot{\theta}_{m_1}, \theta_1, \dot{\theta}_1, \theta_2, \dot{\theta}_2, \theta_{m_2}, \dot{\theta}_{m_2} \right\}^T$.
The non-linear behavior of the dynamic model is analyzed by exciting the system at input T_{m_1} with an odd-odd multisine. Which excites the system at the frequency lines $f_l = 4k+1$ with $k \in \mathbb{Z}$. Then it is possible to show the odd and even nonlinearities as explained by amongst others [9]. Fig. 3 shows that the level of nonlinearity increases with an increasing deflection angle β. Therefore, nonlinear behavior is expected to have an important impact during the state estimations.

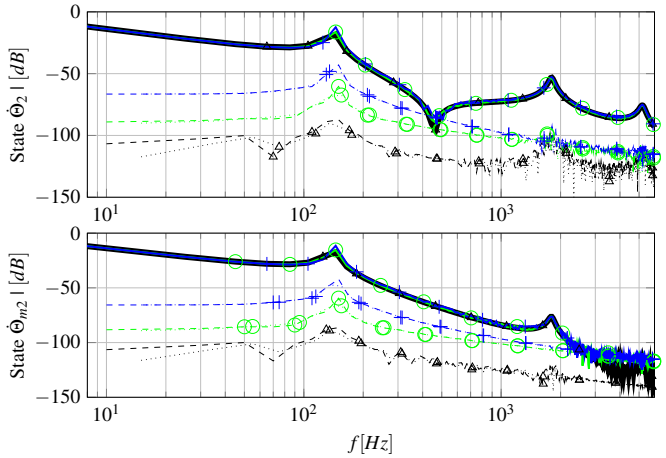

Figure 3 – Measure of even (– – –) and odd (·····) nonlinearities together with the FRF with also odd nonlinearities (———) for different deflection angles β of model 1. ($\triangle$ $\boldsymbol{\beta_1 = \beta_2 = 0°}$, $\circ \beta_1 = \beta_2 = 10$, $+$ $\beta_1 = \beta_2 = 20°$)

3.2. Model induction motor

The induction motor is considered symmetric and without non-linear magnetic material behaviour. Furthermore, higher order harmonics of the magnetomotive force and possible sloped bars are excluded from the model given and elaborated by [10]. This results in the model equation:

$$\dot{\mathbf{x}}_e = \mathbf{A}(\omega_r)\mathbf{x}_e + \mathbf{B}\mathbf{u}, \tag{7}$$

where ω_r equals the angular velocity of the rotor. The state vector $\mathbf{x}_e$ of the electric motor equals $\{i_{sd}, i_{sq}, i^s_{rd}, i^s_{rq}\}^T$. Furthermore, the equations of the induction motor are described in an arbitrary reference frame qd which rotates at $\omega = 100\pi$ $^{rad}/_{s}$. Table 1 summarizes the parameters of the induction motor from the test rig.

3.3. Electro-mechanical system level model

The electric and mechanical models are coupled by concatenation of both sub-model states. The link between both models is made by:

1. the electromagnetic torque T_{em} that drives the mechanical model:

$$T_{em} = \frac{3}{2} p L_m \left(i_{sq} i^s_{rd} - i_{sd} i^s_{rq} \right), \tag{8}$$

with p the number of pole-pairs, L_m the main inductance and i the stator and rotor currents in a qd decomposition[1].

2. the angular velocity $\dot{\theta}_{m_2}$ from the mechanical model which equals the rotor speed ω_r of the electric model.

This model can be employed in a system-level state-estimator which can act as a virtual sensor.

4. MODEL BASED ESTIMATOR

An estimator gives a stochastic estimate of the full state $\mathbf{x}$ of an observed system Σ_O:

$$\begin{cases} \dot{\mathbf{x}}(t) & = \mathbf{f}(\mathbf{x}(t), \mathbf{u}(t), t) \\ \mathbf{y}(t) & = \mathbf{h}(\mathbf{x}(t), \mathbf{u}(t), t) \end{cases}, \tag{9}$$

given the inputs $\mathbf{u}$ and outputs $\mathbf{y}$ of this system. The equivalent discrete-time system of Σ_O is given by

$$\begin{cases} \mathbf{x}[k+1] & = \mathbf{f}_d(\mathbf{x}[k], \mathbf{u}[k], k) \\ \mathbf{y}[k] & = \mathbf{h}_d(\mathbf{x}[k], \mathbf{u}[k], k) \end{cases}. \tag{10}$$

The virtual sensor in this work exploits the Unscented Kalman filter (UKF). This nonlinear Kalman filter propagates the estimated state $\hat{\mathbf{x}}$, which is a random variable, through the (non-linear) system $\mathbf{f}_d$ and measurement $\mathbf{h}_d$ equation of the system model by an unscented transformation (UT). The UT uses a set of $2n+1$ sigma-points $\mathscr{X}_i \in \mathbb{R}^n$:

$$\begin{cases} \mathscr{X}_0 & = \hat{\mathbf{x}} \\ \mathscr{X}_i & = \hat{\mathbf{x}} + \xi \left(\sqrt{\mathbf{P}} \right)_{:i}, & i = 1, \cdots, n \\ \mathscr{X}_i & = \hat{\mathbf{x}} - \xi \left(\sqrt{\mathbf{P}} \right)_{:i}, & i = n+1, \cdots, 2n \end{cases}, \tag{11}$$

where $\left(\sqrt{\mathbf{P}} \right)_{:i}$ is the i^{th} column of the Cholesky decomposition of the dispersion matrix of the random variable. The factor ξ is a scaling factor matching with the weighting factors. The sigma-points describe the argument (a random variable) of a non-linear transformation. Each sigma-point is propagated through the (non-linear) system in the UT and the image of all the sigma-points describes the image of a propagated random variable. The UKF with the UT is discussed in detail in by [11], [12] and [13].

An optimal trade-off between the predictive model covariance (process noise) and the measurement covariance (measurement noise) is key in Kalman-based estimator techniques. The true process noise, which consists of structural and parametric uncertainties for this mechatronic powertrain, is often not normally distributed [14]. Different techniques exist to determine a good approximation of the process noise. The technique developed by [15] is applied in a simplified form here.

The process noise $\mathbf{w}[k]$ is assumed to be symmetric, time invariant and fully resulting from parametric uncertainties (even though input uncertainties will also have an influence in this application). A Monte Carlo simulation is performed to approximate the covariance of the process noise $\mathbf{Q}$. First of all, an arbitrary chosen normal distribution with a variance of 1% of the parameter value is assigned to each parameter p_j. Fifty random parameter sets are constructed based on this distribution. One realization i for each parameter p_j forms $\mathbf{p}^i$.

[1] ^{,s} represent a quantity transformed to the stator

Table 1 – Electrical parameters for the induction motor.

		Stator $\bullet_s$	Rotor $\bullet_r$
r	$[\Omega]$	0.250	0.341
L_σ	$[mH]$	5.0	6.8
L_m	$[H]$	0.2	0.2
p	$[/]$	1	1

The process noise $\mathbf{w}[k]$ is determined at some time steps of a reference simulation by (12). The distribution of the i values for an element of the vector $\mathbf{w}[k]$ is approximated with a normal distribution.

$$\mathbf{w}^i[k] = \mathbf{f}_d\left(\hat{\mathbf{x}}[k], \mathbf{u}[k], \mathbf{p}^i\right) - \mathbf{f}_d\left(\hat{\mathbf{x}}[k], \mathbf{u}[k], \mathbf{p}_{nom}\right) \tag{12}$$

The variance of each element of $\mathbf{w}[k]$ for all the parameter cases i are the diagonal elements of $\mathbf{Q}[k]$, which are shown in figure 4(a). Since the magnitude of Q_{ii} is relatively constant in function of time, the assumption of a time

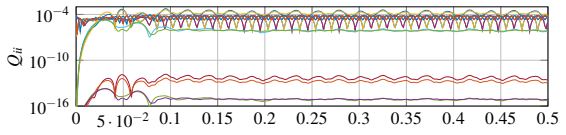

(a) Diagonal elements of $\mathbf{Q}$

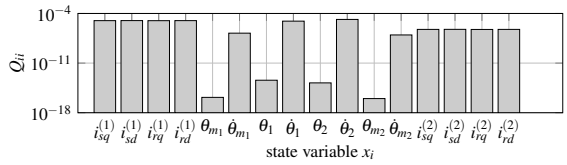

(b) Average $\mathbf{Q}$

Figure 4 – Calculation of $\mathbf{Q}$ for an constantly loaded drivetrain which changes the direction of motion.

invariant process noise covariance will not lead to large errors in this working condition. Other operating conditions have been tested with similar results. Figure 4(b) shows the mean of $Q_{ii}[k]$ and shows that states of the same type of quantity (current, angular position or angular velocity) have a Q_{ii} of the same order of magnitude. Therefore Q_{ii} is subdivided into three groups with the same process noise covariance, namely $Q_i = 10^{-6}$, $Q_\theta = 10^{-5}$ and $Q_{\dot{\theta}} = 10^{-14}$. It should be noted that these values depend on the arbitrary assumed variance of the parameters. However, this analysis provides insight in the mutual relationship between the process noise of the different state. Experimental tests have moreover shown that the UKF is much more robust with respect to the exact choice of these covariances that the extended Kalman filter and performs well with these precomputed values.
Measurement noise values are obtained from the measured noise without excitation on the different sensors.

5. OBSERVABILITY

A given system described by Eq. (9) is observable if the initial state $\mathbf{x}_0$ can be reconstructed from the available outputs $\mathbf{y}$. Many definitions have been discussed in literature , e.g. by [16]. A system should be observable to allow for the state estimator to converge to the state of the observed system.

5.1. Observability rank condition

A system is short time, locally observable (see [16]) if the rank of the observability matrix $\mathscr{O} \in \mathbb{R}^{(k+1)m \times n}$:

$$\mathscr{O}(\Sigma) = \begin{bmatrix} \frac{\partial \mathbf{h}(\mathbf{x})}{\partial \mathbf{x}} \\ \vdots \\ \frac{\partial L_{\mathbf{f}}^k(\mathbf{h})(\mathbf{x})}{\partial \mathbf{x}} \end{bmatrix}, \tag{13}$$

equals the order of the system n [17] for m sensors. The Lie derivatives $L_{\mathbf{f}}^k(\mathbf{h})(\mathbf{x})$, which are the time derivatives of the outputs as described by [18], are:

$$L_{\mathbf{f}}(\mathbf{h})(\mathbf{x}) = \frac{\partial \mathbf{h}(\mathbf{x})}{\partial \mathbf{x}} \mathbf{f}(\mathbf{x}) \tag{14}$$

$$L_{\mathbf{f}}^k(\mathbf{h})(\mathbf{x}) = \frac{\partial L_{\mathbf{f}}^{k-1}(\mathbf{h})(\mathbf{x})}{\partial \mathbf{x}} \mathbf{f}(\mathbf{x}) \tag{15}$$

The in general undetermined value $k \in \mathbb{N}$ to prove unobservability makes this method a sufficient condition for observability, as discussed by [17], [19], [20].

5.2. Popov-Belevitch-Hautus criterium

The Popov-Belevitch-Hautus (PBH) criterion calculates the observability for every mode of the system. The system is observable if the rank of the PBH matrix $\mathscr{O}_{PBH}$:

$$\mathscr{O}_{PBH} = \begin{bmatrix} s\mathbf{I} - \mathbf{A} \\ \mathbf{C} \end{bmatrix}, \tag{16}$$

equals the order of the system n for every eigenfrequency. The matrices $\mathbf{A}$ and $\mathbf{C}$ are calculated by linearization of the system in the examined state:

$$\mathbf{A} = \frac{\partial \mathbf{f}(\mathbf{x}, \mathbf{u})}{\partial \mathbf{x}} \qquad \mathbf{C} = \frac{\partial \mathbf{h}(\mathbf{x})}{\partial \mathbf{x}} \tag{17}$$

The PBH analysis quantifies the observability by calculating the condition κ of $\mathscr{O}_{PBH}$. The influence of each measured state is analysed by starting with a sensor set $\mathscr{S}_0 = \mathbf{x}$ and quantifying the observability for each deleted state measurement. The measured state with the smallest negative effect on the observability upon removal is excluded from the next sensor set. This procedure is applied recursively, and leads to a better quantitative evaluation of the selected sensor set, as also discussed by [21] and [22].

The measure Υ is defined by:

- The n condition numbers $\kappa[\mathscr{O}_{PBH}(\lambda_i, t)]$ for the n system poles at one time step are reduced to one number by the RMS value.
- This measure is inverted to express the observability instead of the unobservability.
- Subsequently, the obtained time signal is reduced to one number Υ by RMS. Furthermore $\underline{\Upsilon}$ and $\bar{\Upsilon}$ are the minimal and maximal value of this obtained time signal.

The "smallest negative effect on the observability upon removal" is specified as the largest $\underline{\Upsilon}$ upon one-by-one removal of all sensors.

5.3. Mechatronic powertrain observability

The observability of the mechatronic powertrain model is first analysed with the rank condition for following five sensor sets:

$$\mathscr{S}_1 = \{i_{sq}^{(1)}, i_{sd}^{(1)}, \theta_{m_1}, \dot{\theta}_{m_1}, \theta_{m_2}, \dot{\theta}_{m_2}, i_{sq}^{(2)}, i_{sd}^{(2)}\} \tag{18}$$

$$\mathscr{S}_2 = \{i_{sq}^{(1)}, i_{sd}^{(1)}, \theta_{m_1}, \dot{\theta}_{m_1}, i_{sq}^{(2)}, i_{sd}^{(2)}\} \tag{19}$$

$$\mathscr{S}_3 = \{i_{sq}^{(1)}, i_{sd}^{(1)}, \theta_{m_1}, \theta_{m_2}, i_{sq}^{(2)}, i_{sd}^{(2)}\} \tag{20}$$

$$\mathscr{S}_4 = \{i_{sq}^{(1)}, i_{sd}^{(1)}, \dot{\theta}_{m_1}, \dot{\theta}_{m_2}, i_{sq}^{(2)}, i_{sd}^{(2)}\} \tag{21}$$

$$\mathscr{S}_5 = \{i_{sq}^{(1)}, i_{sd}^{(1)}, \theta_{m_1}, \dot{\theta}_{m_1}\} \tag{22}$$

Table 2 shows that all sensor sets make the complete system observable.

Table 2 – Observability rank for different sensor sets for increasing Lie-derivatives **k**.

k	$\mathscr{S}_1$	$\mathscr{S}_2$	$\mathscr{S}_3$	$\mathscr{S}_4$	$\mathscr{S}_5$
0	8	6	6	6	6
1	14	11	12	12	10
2	<u>16</u>	14	14	14	12
3		<u>16</u>	<u>16</u>	<u>16</u>	14
4					<u>16</u>

However, a quantitative PBH observability analysis shows that some of these sets lead to very poor observability properties, which will in turn lead to very poor noise attenuation. The removal of four sensors from the full state measurement $\mathscr{S}_0$ is motivated by the analysis of Υ for the removal of different sensors, given in Fig. 5.

This figure shows the redundancy in multiple angle measurements. It follows from other PBH analyses that the location of the single necessary angle measurement is not significant. The pragmatic location is at the rotor of the induction motor. In the same manner, it can be shown that the rotor currents should not be measured to obtain observability. After the removal of the rotor currents, three angular velocity sensors can also be removed from the set. At this point, the observability $\underline{\Upsilon}$ lowers several orders of magnitude. The location of the remaining angular velocity sensor is again not significant.

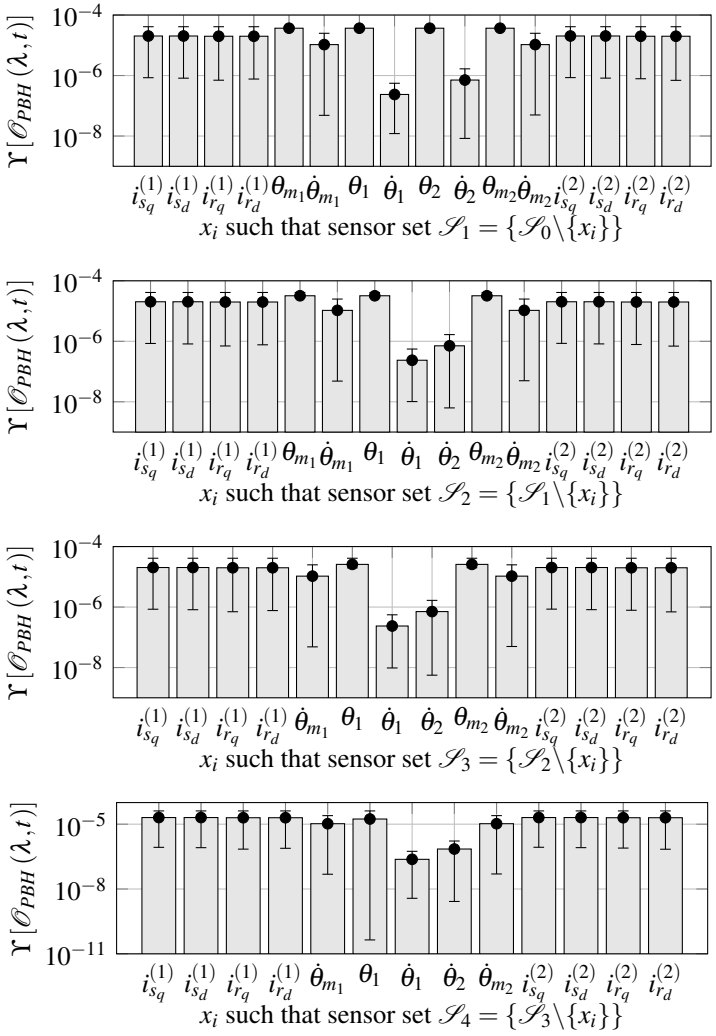

Figure 5 – $\Upsilon[\mathscr{O}_{PBH}]$ in a loaded standstill condition of the drivetrain. Υ, $\underline{\Upsilon}$ and $\bar{\Upsilon}$ are shown as respectively a bar, the lower and upper marking.

The sensor sets from Eq. (18)-(22) are all observable according to the rank criterion. However, the quantified observability becomes very low if all current measurements from one induction motor are missing. The influence of the sensor set can be further examined based on the estimation error.
The influence of the sensor sets $\mathscr{S}_1$ to $\mathscr{S}_5$ on the predictive estimation error[2] $\mathscr{E}$ is also analyzed. The estimation errors $\tilde{x}_i(t) - \hat{x}_i(t)$ are reduced to one relative error at each time step by introducing $\mathscr{E}$. The error $\mathscr{E}$ is the RMS value of the relative error $\tilde{x}_i - \hat{x}_i$ with respect to the RMS value of $\hat{x}_i$. The estimation errors for the states of which the measurements are not used, is shown in figure 6. This figure clearly shows that the predicitive error is relatively

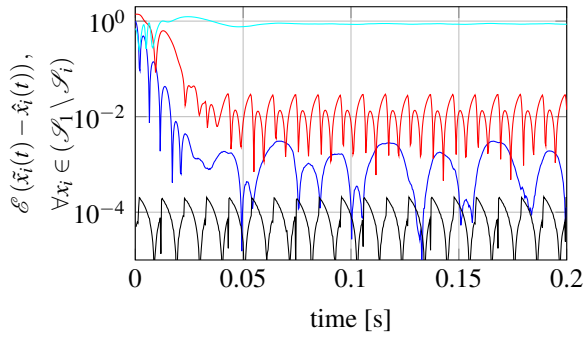

Figure 6 – Predictive estimation error $\mathscr{E}$ for different sensor sets at a nominal speed of 1200 rpm and an approximately constant load.

good for all measurement sets except for the $\mathscr{S}_5$ set.
It is now also interesting to consider the actual error (without the normalisation of $\mathscr{E}$). The absolute errors on the angular position and velocity of the second induction motor are shown in Fig. 7.

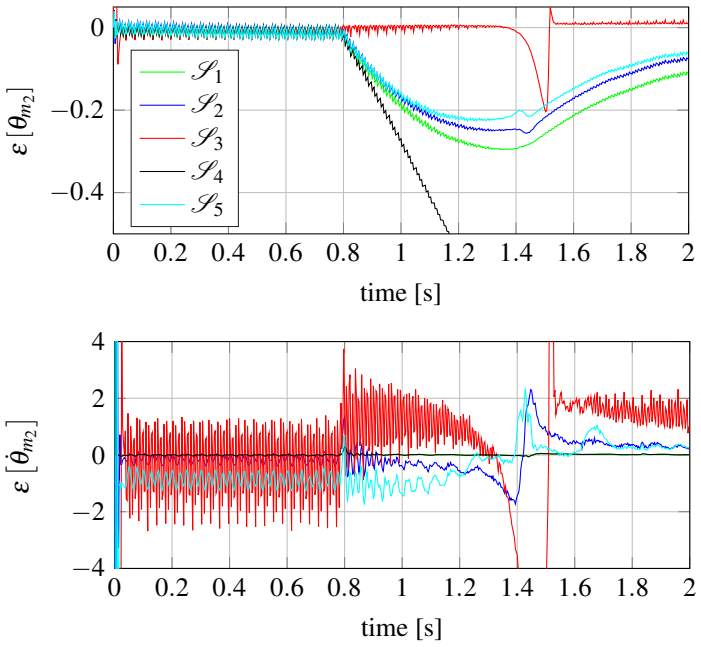

Figure 7 – Estimation error $\varepsilon\left[\theta_{m_2}\right]$ and $\varepsilon\left[\dot{\theta}_{m_2}\right]$ with the same conditions and settings of figure 6.

Even though the velocity is estimated very well for $\mathscr{S}_4$, this is not a good measurement set as the error for the angular position becomes relatively large. From this analysis measurement set $\mathscr{S}_2$ would be selected as it provides similar accuracy as $\mathscr{S}_1$ but with one less sensor. A virtual sensor with the presented system level model and measurement set $\mathscr{S}_2$ is therefore concluded to provide accurate results for real-world applications.

[2]The predictive error is obtained by comparing the estimates with measurements $\tilde{\bullet}$, which were not used for the estimator.

6. CONCLUSION

This work presents the development and validation of a virtual sensor for mechatronic powertrains. This work discusses the multiphysical model for this system and how this integrates with nonlinear Kalman filters. A Monte Carlo simulation is used in order to determine the Kalman filter settings. This approach works well on the experimental tests performed by the authors. For practical virtual sensors, a minimal instrumentation is highly desirable. We therefore performed a detailed observability study to analyze the necessary and preferable sensorization. The accuracy for the resulting virtual sensor is tested by considering the predictive error, which is the difference between the estimated states and the unused sensors on a test setup. This show good accuracy for the proposed approach. Further research will focus on the exploitation of commercial system level modeling tools, like LMS Imagine.Lab Amesim, in order to set up more general mechatronic models for virtual sensors.

ACKNOWLEDGEMENTS

The research of W. Rottiers and F. Naets is funded by a grant from the Research Foundation - Flanders (FWO). The Research Fund KU Leuven is also gratefully acknowledged for its support. This work also benefits from the Belgian Programme on Interuniversity Attraction Poles, initiated by the Belgian Federal Science Policy Office (DYSCO). The Flanders Innovation & Entrepreneurship Agency within the ECOPOWERTRAIN project is gratefully acknowledged for its support. This research was partially supported by Flanders Make, the strategic research centre for the manufacturing industry, through the MOFORM project.

REFERENCES

[1] Albertos, P., Goodwin, G.C., “Virtual sensors for control applications”, Annual Reviews in Control, 26(1), 2002, pp. 101–112.

[2] Gauthier, J., Hammouri, H., Othman, S., “A simple observer for nonlinear systems applications to bioreactors”, 37(6), 1992, pp. 875–880.

[3] Petersen, C.D., Fraanje, R., Cazzolato, B.S., Zander, A.C., Hansen, C.H., “A Kalman filter approach to virtual sensing for active noise control”, Mechanical Systems and Signal Processing, 22(2), 2008, pp. 490–508.

[4] Oosterom, M., Babuska, R., “Virtual sensor for fault detection and isolation in flight control systems-fuzzy modeling approach”, Proceedings of Decision and Control, 2000. Proceedings of the 39th IEEE Conference on, vol. 3, IEEE, 2000, pp. 2645–2650.

[5] Henningsson, M., Tunestål, P., Johansson, R., “A virtual sensor for predicting diesel engine emissions from cylinder pressure data”, vol. 45, Elsevier, 2012, pp. 424–431.

[6] Cheng, J.W.J., Chao, T.C., Chang, L.H., Huang, B.F., “A model-based virtual sensing approach for the injection molding process”, Polym Eng Sci, 44(9), 2004, pp. 1605–1614.

[7] Forrier, B., Naets, F., Desmet, W., “Virtual sensing on mechatronic drivetrains using multiphysical models”, 2015.

[8] Seherr-Thoss, H.C., Schmelz, F., Aucktor, E., Universal joints and driveshafts analysis, design, applications, Springer, 2006.

[9] Lampaert, V., Swevers, J., Al-Bender, F., “Impact of nonlinear friction on frequency response function measurements”, Proceedings of Proceedings of the international seminar on modal analysis, vol. 1, KU Leuven; 1998, 2001, pp. 443–450.

[10] Krause, P.C., Analysis of electric machinery and drive systems, IEEE Press power engineering series, IEEE Press, 2nd ed ed., 2002.

[11] Simon, D., Optimal State Estimation: Kalman, H Infinity, and Nonlinear Approaches, Wiley-Interscience, 1 edition ed., 2006.

[12] Van Merwe, R.D., Wan, E.A., Julier, S.I., “Sigma-point kalman filters for nonlinear estimation and sensor-fusion - Applications to integrated navigation”, Proceedings of Collection of Technical Papers - AIAA Guidance, Navigation, and Control Conference, 2004.

[13] Julier, S., Uhlmann, J., Durrant-Whyte, H., “A new method for the nonlinear transformation of means and covariances in filters and estimators”, IEEE Transactions on Automatic Control, 45(3), 2000, pp. 477–482.

[14] Salau, N.P., Trierweiler, J.O., Secchi, A.R., Marquardt, W., “A new process noise covariance matrix tuning algorithm for Kalman based state estimators”, Proceedings of 7th IFAC International Symposium on Advanced Control of Chemical Processes, vol. 7, 2009.

[15] Valappil, J., Georgakis, C., “Systematic estimation of state noise statistics for extended Kalman filters”, 46(2), 2000, pp. 292–308.

[16] Hermann, R., Krener, A.J., “Nonlinear controllability and observability”, IEEE Transactions on Automatic Control, 22(5), 1977, pp. 728–740.

[17] Krener, A.J., Ide, K., “Measures of unobservability”, Proceedings of Proceedings of the 48th IEEE Conference on Decision and Control, 2009 held jointly with the 2009 28th Chinese Control Conference. CDC/CCC 2009, 2009, pp. 6401–6406.

[18] Hinson, B.T., “Observability-Based Guidance and Sensor Placement”, 2014.

[19] Anguelova, M., “Nonlinear Observability and Identifiability: General Theory and a Case Study of a Kinetic Model”, 2004.

[20] De Wit, C., Youssef, A., Barbot, J.P., Martin, P., Malrait, F., “Observability conditions of induction motors at low frequencies”, Proceedings of Proceedings of the 39th IEEE Conference on Decision and Control, 2000, vol. 3, 2000, pp. 2044–2049 vol.3.

[21] Salau, N.P., Trierweiler, J.O., Secchi, A.R., “Observability analysis and model formulation for nonlinear state estimation”, Applied Mathematical Modelling, 38(23), 2014, pp. 5407–5420.

[22] Tamarozzi, T., Risaliti, E., Rottiers, W., Desmet, W., et al., “Noise, ill-conditioning and sensor placement analysis for force estimation through virtual sensing”, Proceedings of International Conference on Noise and Vibration Engineering (ISMA2016),, 2016.